JOURNAL OF PROPULSION AND POWER
Vol. 13, No. 1, January–February 1997

Unsteady Flow and Shock Motion in a Transonic Compressor Rotor

W. W. Copenhaver* and S. L. Puterbaugh†
U.S. Air Force Wright Laboratory, Wright–Patterson Air Force Base, Ohio 45433
and
C. Hah‡
NASA Lewis Research Center, Cleveland, Ohio 44135

The results of an experimental and numerical comparison of the unsteadiness and shock motion that occurs in the tip region within a modern, low-aspect-ratio, high-through-flow, axial-flow transonic fan rotor are presented. The unsteadiness studied here is associated with local phenomena within the blade passage and not related to blade row interaction. Unsteady static pressures were measured at the casing over the rotor that operates at a tip relative Mach number of 1.6. An unsteady three-dimensional Navier–Stokes computational study was performed with tip clearance comparable to the test rotor. The fully three-dimensional, unsteady, Reynolds-averaged Navier–Stokes equations were solved with time steps, each nominally of 2.8×10^{-5} s in duration or approximately five times blade pass frequency. The results in the clearance gap were retained from the computational solution and compared with the experimental measurements. Both indicated deterministic unsteadiness near the location of the shock. High levels of unsteadiness were also measured downstream of the shock in the path of the clearance vortex, but this phenomenon was not predicted by the computation. The unsteadiness near the shock was shown to be a result of movement of the shock. The amplitude and frequency of shock position oscillation was estimated from the results to be about 2% chord and 2 kHz, respectively. Analysis of loss caused by the shock unsteadiness suggested that losses because of shock motion were insignificant relative to the steady shock loss at the relative Mach number studied.

Introduction

TO meet the performance requirements of advanced military engines, fans must be developed that deliver high levels of efficiency. However, large efficiency reduction occurs in the tip region of transonic, unshrouded fan rotors. This is because of the presence of and mutual interaction between the clearance flow, core flow, boundary layers, and shocks. Though these structures and their relationship to loss can be evaluated in a steady or Reynolds-averaged state, their unsteady nature has been suggested to contribute to the production of loss. Kerrebrock[1] observed that a correlation exists between increased loss and increased unsteadiness when nearing the tip region in a spanwise sense. This is the unsteadiness that is generated within the blade row itself and independent of the unsteadiness generated by blade row interactions.

Most investigations to date have only addressed the steady nature of the tip flowfield.[2–6] However, several experimental studies have investigated the unsteadiness as related to shock movement. Strazisar[7] measured shock motion of 3.5% of chord from laser anemometer data. He estimated that for a shock frequency of 1 kHz this motion will produce an increase of 11% in shock loss relative to a stationary shock. Ng and Epstein[8] studied flowfield unsteadiness via measurements at the exit of a transonic fan rotor. Fluctuations were found at three to four times the blade pass frequency (15–20 kHz), with amplitudes as large as the wake total pressure defect at the tip. It was postulated that these fluctuations were attributed to shock motion in the rotor-relative reference frame, which could be caused by relaxation oscillations with the boundary layer or von Kármán vortex streets shed in the blade wakes. Hathaway et al.[9] confirmed that the rotor blade vortex shedding frequency was in the range of 15–20 kHz, and therefore, may drive the shock oscillations seen by Ng and Epstein.[8] Alday et al.[10] found in two axial flow transonic rotors that flow near the rotor tip, where the highest losses were occurring, was extremely random in nature.

These studies have demonstrated the importance of understanding the unsteady aspect of the tip flowfield when exploring loss generation. In the studies just cited, transonic tip flowfield phenomena have been explored with relatively simple computational models, which may not capture all of the relevant interactions, such as shock boundary-layer interaction and shock-clearance flow interaction. Computational capability has improved to the point where a fully three-dimensional, viscous, unsteady analysis is now possible. Relatively few unsteady numerical studies have been reported in the open literature. Owen,[11] Scott and Hankey,[12] and Epstein et al.[13] studied unsteady flow phenomena inside a two-dimensional cross section of a transonic compressor. However, the flow phenomena that occur in highly loaded compressor configurations cannot be fully investigated using a two-dimensional assumption. Recently, various unsteady flow analyses have been reported for the simulation of multiple blade row interactions.[14–19] However, these studies mainly investigated flow unsteadiness caused by the physical interaction of flowfields of adjacent blade rows.

The current study attempts to explore the state of the art in computational capability with regard to unsteady transonic compressor rotor tip flowfields for an isolated rotor where the primary source for unsteadiness would be the passage shock

Received Aug. 10, 1995; revision received May 17, 1996; accepted for publication May 20, 1996.

*Aerospace Research Engineer, Aeropropulsion and Power Directorate, POTF, Building 18, 1950 Fifth Street. Senior Member AIAA.

†Aerospace Engineer, Aeropropulsion and Power Directorate, POTF, Building 18, 1950 Fifth Street. Member AIAA.

‡Senior Scientist, Internal Fluid Mechanics Division, 21000 Brookpark Road, M/S 5-11. Member AIAA.

system. In the study, the influence of the stator on the rotor has been eliminated only to simplify the task of code assessment. Certainly the stator would influence the rotor in an unsteady fashion and this must be considered in future studies, but the goal of this study is to first establish the computational capabilities on the isolated rotor. The study will also expand on the knowledge base of unsteady interactions in transonic compressors through experimental results. In this article, the authors do the following:

1) Present new experimental evidence of transonic rotor tip unsteadiness at two design speed operating conditions.

2) Compute the unsteady flowfield for the rotor using a fully three-dimensional unsteady Reynolds-averaged Navier–Stokes analysis.

3) Identify the unsteady flow structures present in transonic rotor tips.

4) Discuss some implications of the computational and experimental comparison on future improvements to computational capabilities and experimental methods.

Experiment

Test Article

A schematic diagram of the compressor test rig is shown in Fig. 1. Note that there are no inlet guide vanes or upstream struts in this test configuration. Details of the test facility and steady-state instrumentation are provided by Law and Wadia[20] and Copenhaver et al.[21]

The rotor used for the current work, denoted rotor 4, is a low-aspect-ratio, high-through-flow, highly loaded configuration. Detailed design information on rotor 4 was provided by Parker and Simonson.[22] The rotor overall performance was studied in detail by Copenhaver et al.[21] and Wadia and Copenhaver.[23] The stator configuration was designed through a computational fluid dynamics technique as was reported by Copenhaver et al.[21]

The peak efficiency stage performance with rotor 4 installed along with some geometric information is given in Table 1.

Measurements

The tip flowfields of transonic rotors have been studied both experimentally and computationally by many authors.[24–29] It is somewhat surprising to note that little if any rotor-relative unsteady information concerning the tip flowfield in the cascade plane of a transonic rotor is found in the open literature. Most presentations of unsteadiness include rotor exit information. One possible reason is that, since the time history of the signals must be simultaneously retained for multiple transducers, the data storage requirements are imposing and handling such data sets has been quite difficult until comparatively recent advances in computer mass storage and networking.

For this study, high-response casing-mounted pressure transducers were used to measure the blade tip static pressure distribution. Details of the ensemble-averaged static pressure measurements were reported by Sellin et al.[30] In summary, the 10 casing-mounted transducers used to measure the time-resolved static pressures were evenly spaced in the region extending from 40% of the axial chord projection upstream of the leading edge to 80% downstream of the leading edge. Transducer sensing surface diameters were 0.073 in. (1.77% blade chord). The distribution of the transducers relative to the rotor is shown graphically in Fig. 2. Measurement density was limited because of the physical requirements for transducer placement. Although a higher measurement density would be desired, the density is adequate to identify the dominant structures and locate and quantify areas of high unsteadiness.

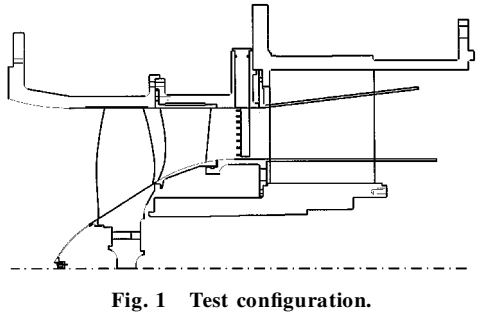

Fig. 1 Test configuration.

Table 1 Test article parameters

Pressure ratio,[a] 2.047
Isentropic efficiency, 90.4%
Corrected flow per annulus area, 43.38 lbm/s-ft^2
Corrected tip speed, 1500 ft/s
Approximate inlet tip relative Mach number, 1.6
Mean rotor aspect ratio, 1.320
Rotor inlet hub/tip ratio, 0.312
Mean tip clearance (% of tip chord), 0.6%
Approximate design blade pass frequency, 7 kHz
Blade count, 20

[a]Reference data point no. srs93042012.

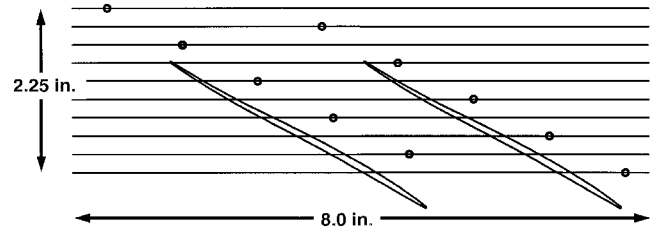

Fig. 2 Transducer locations.

Transducer Calibration and Measurement Uncertainty

The design of the test rig (Fig. 1) allowed the pressure transducers to be calibrated in place. With the rotor removed, known pressures were applied to each of the casing-mounted pressure transducers. Since the transducer output is linear in the pressure range of interest, a two-point calibration was performed, with pressures of atmospheric and 10 psig.

A measurement uncertainty analysis was performed for a representative discrete value of the unsteady pressure signal, which included the effect of all components involved in measurement and calibration. The bias error was estimated to be ± 0.05 psi and the precision error was estimated to be ± 0.07 psi. This gave an overall uncertainty of ± 0.086 psi at a 95% confidence interval. The significance of the unsteadiness information could, of course, be compromised by excessive measurement uncertainty. In particular, the precision error component has a direct bearing if it is assumed that the bias error changes little over the recording period, which is a reasonable assumption. The threshold below which unsteadiness would be considered insignificant was computed to be equivalent to a precision error of ± 0.07 psi. Root mean square magnitudes well over this value were seen in each test case.

Data Processing

The data were digitized from previously recorded analog tape and further processed by software. The digital sampling rate was set at (279 kHz), thereby providing 40 samples to span one blade passage. A once-per-revolution synchronization signal was used to phase lock the signals during processing. This allowed the rotor to be phase-locked such that subsequent ensemble averaging and unsteadiness calculations would be done for the same blade passage on each revolution. It was determined that an average of 125 ensembles from each transducer output was required to obtain an adequate steady-state representation of the macroscopic tip flow structure. Root mean square levels were obtained by comparing all 125 ensembles with the average, for the blade passage analyzed.

The nature of the laboratory frame-fixed position of the casing mounted transducers limits the information that is obtainable. Rotor relative frame static pressure information that is presented later will indicate the nonengine order variation in static pressure. Variations that are integral multiples of the once-per-revolution rotor frequency are not detected. The rotor potential field will be included in the measurements, but it is not possible to resolve the influence of the nature of the stator potential field in the rotor relative frame, since the position of the transducers relative to the stator row is fixed. Therefore, the potential field influence of the stator on the rotor is constant in the measurements presented.

Since the 10 casing measurements are made at different axial/circumferential locations (Fig. 2), the stator field pitchwise influence is slightly different for each measurement. However, the relative positions of the transducers and stator vanes are fixed. Therefore, when the rotor is in a given position, the instantaneous, ideal potential field influence of the rotor and stator on a given measurement is the same from revolution to revolution. (The effective sampling rate of the dynamic measurement is once per revolution.) Consequently, the influence of the stator potential field on the measurements is minimal with regard to unsteady comparisons.

Numerical Methods

The present study aims to solve numerically the unsteady flowfield for rotor 4 in isolation. The numerical component is intended to identify the causal relationships between the locally generated unsteadiness and shock motion near the tip region. A three-dimensional steady Navier–Stokes code that has been successfully tested for a wide range of turbomachinery flows was extended to execute a time-accurate calculation.[31] The steady computation was extensively compared with steady experimental measurements for rotor 4 at peak efficiency by Copenhaver et al.[21] and Puterbaugh,[32] showing good agreement. The steady solution was obtained first with a large effective time step. The converged steady solution was then used as an initial condition for the unsteady computation. At each time step, the overall residual is reduced by four orders of magnitude from the initial value.

During the development of a time-accurate calculation, it was found that high-order discretization schemes are necessary for both the space and the time discretization to avoid excessive numerical dissipation. The effects of the turbulent fluctuation are included through the turbulence model. The turbulence is represented through the ensemble-averaged turbulence kinetic energy and turbulence dissipation rate. These two turbulence variables are obtained by solving the unsteady form of the transport equations for the turbulence kinetic energy and the dissipation rate. Low Reynolds number modifications are used and the turbulence variables are integrated up to the wall. A wall function is not used near the solid wall.

For the time-dependent terms, an implicit second-order scheme was used. For this approach, a number of subiterations was performed between each time step. The specific number of subiterations that was determined by the size of the time step was typically 15–20 for the present application. At each time step, the governing equations were solved with an implicit relaxation method using a fully conservative control volume approach. A third-order-accurate interpolation scheme was used for the discretization of the convection terms and central differencing was used for the diffusion terms. The method is of second-order accuracy with smoothly varying grids.

The grid used for this study was a blade centered I-type grid. The I-type grid is a body-fitted, nonperiodic grid characterized by excellent orthogonality, as shown in Fig. 3. For the current study, the grid had 50 nodes in the pitchwise direction, 46 nodes in the spanwise direction, and 151 nodes in the streamwise direction. For the tip region, seven nodes were distributed from the suction to the pressure surface with six nodes in the clearance gap, as demonstrated in Fig. 4.

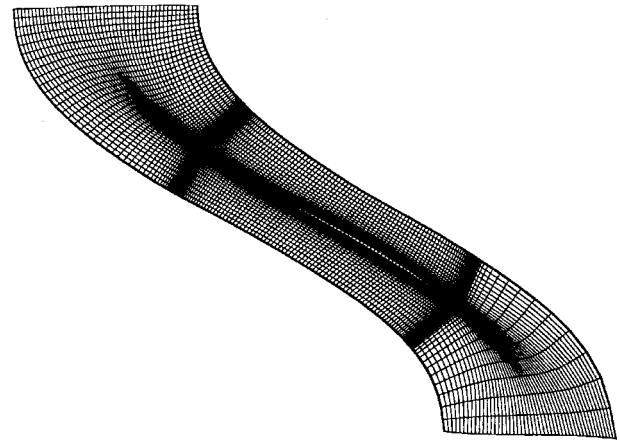

Fig. 3 Blade-to-blade computational grid, tip region.

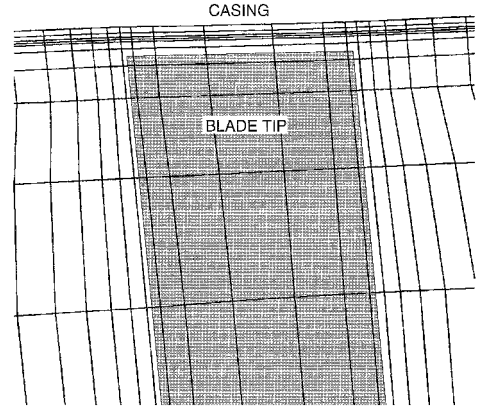

Fig. 4 Tip gap description.

Standard boundary conditions for the current type of problem were imposed. At the inlet, total temperature and the total pressure condition along with two components of velocity vectors were specified. At the exit, the static pressure was imposed at one point. These boundary conditions were applied strictly as nonreflecting conditions to produce physically accurate unsteady results.

Many factors were considered when selecting an appropriate time step for the calculation. The primary considerations for this study were to capture the fundamental frequencies of the shock motion, stay within mass storage restrictions, and maintain numerical stability. The optimum sample rate was selected based upon these considerations, and therefore, may not be ideal for other studies, such as rotor-stator interaction, where higher rates would be required.

Shock motion frequency was estimated based on a simple analysis of the time required for a pressure wave to travel from the shock on the suction surface to the trailing edge and back. The analysis was done by assuming that the wave would travel along a grid line near the blade suction surface. The net velocity was computed as the difference between the local velocity vector and the local speed of sound with direction determined by whether the wave was traveling upstream or downstream. The traveling wave time determined from the steady solution Mach number distributions was 5×10^{-4} s or at a frequency of approximately 2 kHz. Following the Nyquist criterion a sample rate of at least 2.5×10^{-4} would be required to capture this type of wave phenomena. Therefore, the time step for all of the unsteady computations was selected to be nominally 2.8×10^{-5}, representing an effective numerical sample rate of approximately 35.7 kHz or five times rotor blade passing. Time steps greater than this could not be obtained because of numerical stability considerations.

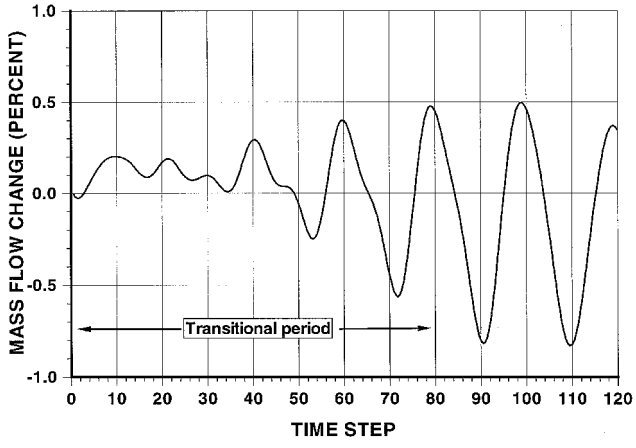

Fig. 5 Mass flow convergence history.

It was necessary to store up to 20 samples at the chosen sample rate for one shock period to be captured. Higher sample rates would require more storage to assess shock motion. The transitional effects on the numerical results were eliminated by running the unsteady computation 160 steps beyond its transition period before making any unsteady observations. Figure 5 demonstrates the mass flow convergence history. The solution requires approximately 80 time steps to transition from steady conditions to a periodic solution where the mass flow fluctuations are on the order of $\pm 0.5\%$ of the starting steady flow and at a frequency of approximately 2 kHz. A total of 160 time steps were analyzed for flowfield details in blocks of 40 to maintain reasonable storage file sizes. Based on the sample rate of 2.8×10^{-5}, 160 time steps establish a low-frequency limit of approximately 225 Hz, below which unsteadiness cannot be resolved.

Results

Experimental and computational results were obtained and compared at the peak efficiency and near-stall operating points at design speed. The test article experienced no rotating stall at the near-stall operating condition. Therefore, the unsteadiness shown in the results at near stall is not related to a stalling condition. The unsteadiness comparisons are primarily based on two-dimensional distributions of the rms variation of static pressure in the blade-to-blade plane near the casing. The experimental rms values were computed from an ensemble of 125 pressure distributions, each covering the same blade pitch, whereas the numerical rms values were computed from an ensemble of 160 blade pitch pressure distributions, or time steps.

Two well-defined areas of deterministic unsteadiness within the blade passage are evident. The first is characterized by shock motion and the second by postshock unsteadiness. These two areas will be compared both qualitatively and quantitatively in subsequent sections.

Shock Motion

Figure 6 shows a comparison of the measured and computed contours of rms static pressure for the tip region of the compressor at near-stall operation. The computations (Fig. 6a) show an area of high unsteadiness just in front of the blade leading edge in a narrow band emanating from the suction surface of the blade and terminating upstream of the blade leading edge. This region coincides with the shock position, which is detached at this near-stall operating point. The unsteadiness dissipates quite rapidly as it extends upstream in a direction normal to the blade chord. This is primarily a result of the change in grid density that exists in the I-grid configuration at the periodic boundary. The true upstream termination point for this unsteadiness cannot be determined with this grid configuration. Peak levels of unsteadiness in this structure exist in the passage directly upstream of the leading edge and

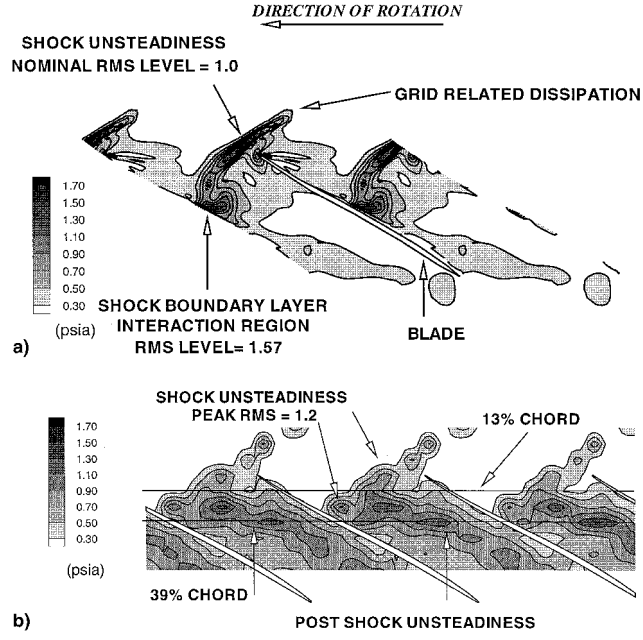

Fig. 6 a) Computed contours of rms pressure fluctuations in clearance region (near stall) and b) measured contours of rms pressure fluctuations on casing wall (near stall).

downstream of the suction surface intersection point. At the shock-suction surface intersection point an increase in unsteadiness can be seen emanating from the surface and extending slightly downstream. The peak rms level in this region is 1.57.

The measurements (Fig. 6b) show the same local peak in unsteadiness near the position of the shock that supports the computational results. The unsteadiness extends upstream as far as the measurements are available and terminates on the suction surface. Just as in the computation, a local peak of unsteadiness appears near the intersection of the shock and the suction surface. The measured rms level in this region was 1.2 psi vs 1.57 psi from the computation.

To provide a more quantitative comparison, the rms variation in static pressure at 13% chord is shown in Fig. 7a. The rms distributions agree well in both level and character. The figure shows a slightly different shock location for measured and computed results. This may be a result of slight differences in back pressure. Figure 7b shows the same comparison at 39% chord. Good agreement in shock rms magnitude is shown, but a significant difference is apparent in the midpassage region behind the shock. The measured postshock unsteadiness is not predicted by the computation. These differences will be discussed further in the postshock unsteadiness section.

The computation has sufficient temporal resolution (2.8×10^{-5} s) and was run at a sufficient number of time steps to establish periodicity. Shock oscillation frequency was determined from the computational results. The evaluation was done by computing the unsteady components of velocity at each time step. The unsteady component is defined as the vector difference between the vector field at a given time step and the steady solution. This representation enhanced the ability to discern flowfield differences between time steps. In the case of shock system motion, the vectors change magnitude and direction as a function of the shock system speed and direction. The vector field was seen to repeat after approximately 18 time steps, which implied a shock oscillation frequency of approximately 2 kHz. This is on the order of six times the rotor rotational frequency (350 Hz) and one-quarter of the blade pass frequency (7 kHz). This is the same frequency that was computed for a pressure disturbance to travel from the shock system to the blade trailing edge and return. This suggests that the oscillation is a result of a pressure-based disturbance with a time scale equivalent to travel to the trailing edge and back.

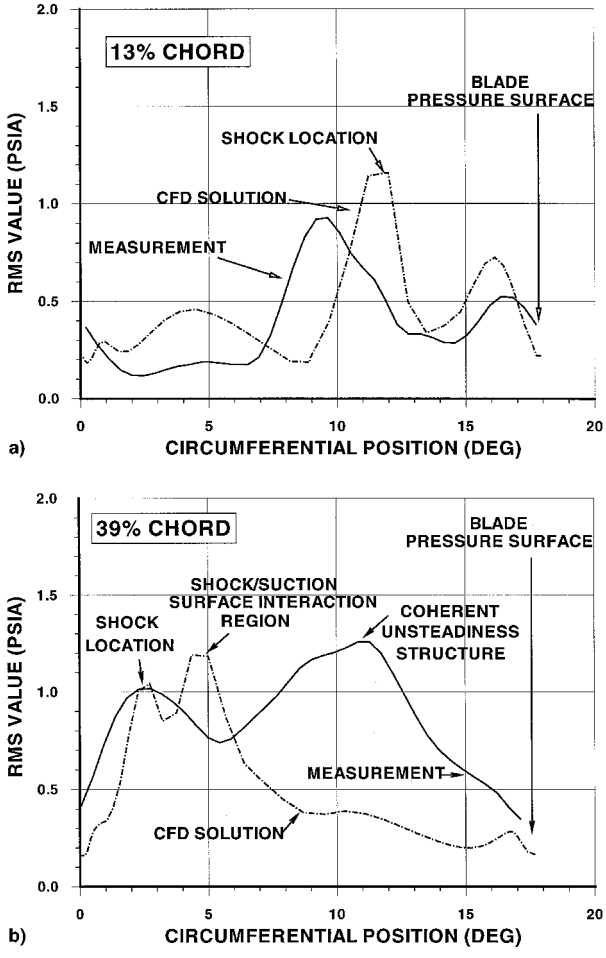

Fig. 7 a) Comparison of measured and computed rms pressure levels (13% blade chord) and b) comparison of measured and computed rms pressure levels (39% blade chord).

In addition, the estimated shock frequency of 2 kHz is of the same order of magnitude as found in some other fundamental internal flow and isolated airfoil studies.[33–35] In each of these studies the shock-boundary-layer interaction was seen to drive shock oscillation.

To further explore shock motion, the movement of the sonic line in the blade passage was determined. The largest movement of the shock within the clearance gap is closest to the blade suction surface region, with a maximum variation of 0.8% of chord. The measured variation in shock position was determined to be about 2.0% of chord. This was done by examining the time history of pressure signals at 13% chord, which represents the mean shock position at about midpassage. The shock is indicated by a sharp pressure rise, whereas the blade is indicated by a sharp pressure drop. The range of shock positions was determined by calculating the time difference between a rise in the signal when crossing a threshold associated with the shock position and a drop in the signal when crossing a threshold associated with the blade position. This was done for each of the 125 pressure distributions measured from the same blade passage. The change in these differencing times, modified appropriately for geometry and time-space scaling, indicates the variation in shock position. Since the time differences were computed from shock-to-blade for each pressure distribution, any influence of errors in blade position is eliminated.

The losses attributed to shock unsteadiness can be estimated following the approach defined by Strazisar.[7] The net shock loss caused by harmonic motion can be determined by computing the shock translational Mach number as a function of frequency and amplitude. This translational Mach number is added to the steady shock Mach number, giving a time history of the shock entrance Mach number. From this information the associated time-resolved pressure loss can be determined. The loss is averaged for one period and compared to the steady shock loss to assess the impact of shock unsteadiness on loss. Figure 8 shows the effect of shock oscillation amplitude and steady normal Mach number on an increase in shock loss for a shock oscillation frequency of 2 kHz. For the conditions at near stall in this study the increase in loss resulting from shock unsteadiness at the rotor tip is approximately 1%. Figure 8 demonstrates the impact of the steady shock Mach number on unsteady loss contributions. At lower Mach numbers shock system unsteadiness has a more significant impact over the steady loss level. From these results, it can be stated that unsteadiness of the shock system in the tip of the rotor studied does not significantly contribute to shock loss. Further study is required to determine the impact of shock unsteadiness on loss because of shock-boundary-layer interaction, shock–vortex interaction, and postshock unsteadiness.

Figure 9 details the comparison of computed and measured rms variation in static pressure at the near peak efficiency operating point. For this operating point the shock system is attached to the blade leading edge and contained within the passage. The computed results (Fig. 9a) indicate unsteadiness primarily at the shock location with the general level being 0.4–0.6 psi. This is approximately one-half the magnitude

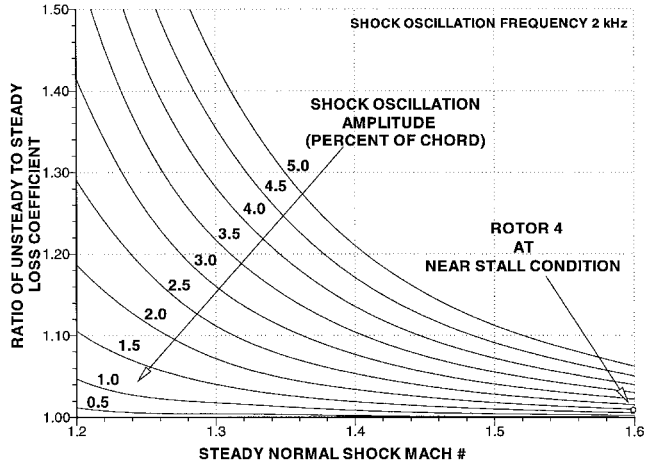

Fig. 8 Impact of shock amplitude and steady Mach number on loss.

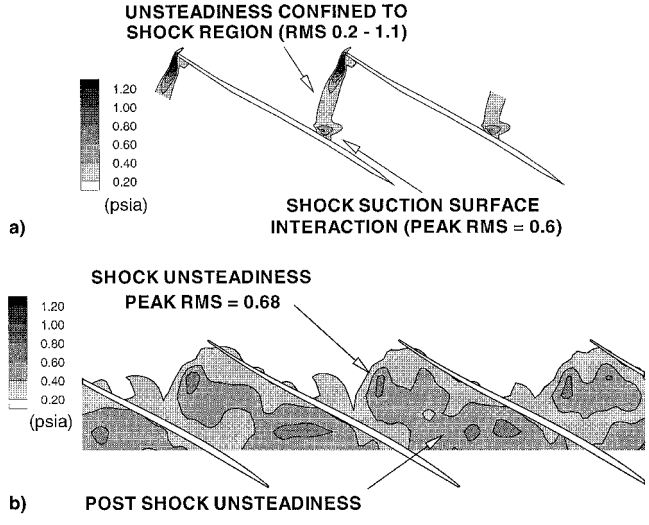

Fig. 9 a) Computed contours of rms pressure fluctuations in clearance region (peak efficiency) and b) measured contours of rms pressure fluctuations on casing wall (peak efficiency).

computed at the near-stall condition. Again, a local peak in unsteadiness exists near the shock–suction surface intersection. The measured results (Fig. 9b) also show unsteadiness confined within the passage with peak levels near the shock of 0.7 psi. This agrees well with the computed levels and also is nearly half the levels seen at near stall. The unsteadiness in measured static pressure persists downstream of the shock and is not captured by the computations.

Although the comparisons in this study are limited to time-resolved static pressures, they do suggest that the computation adequately represent shock motion in this rotor. The measured rms levels of shock motion were predicted within reasonable bounds. These results support the notion that shock system unsteadiness exists within an isolated rotor and that the levels increase substantially when the shock system becomes detached from the leading edge and extend out from the blade passage. The analysis of these results also suggests that shock loss is not increased substantially by the levels of unsteadiness seen in this study.

Postshock Unsteadiness

The area of coherent unsteadiness evident in the measurements downstream of the shock (Fig. 6b and Fig. 9b) is identified as postshock unsteadiness. This area begins near midpitch and migrates toward the pressure surface as it extends downstream as demonstrated by Fig. 6b. Recent work by Puterbaugh[32] and Puterbaugh and Copenhaver[36] suggested that this unsteady structure is the result of the interaction between the clearance flow and the shock. Fundamental studies by Cattafesta[37] on weak shock–vortex interactions in a Mach 2.5 overexpanded freejet showed shock and postshock unsteadiness.

The measured results in Figs. 6b and 9b suggest that, for this rotor, the unsteadiness continues far downstream of the shock to the blade row exit. The region of postshock unsteadiness corresponds very closely to the low-velocity region behind the shock at the rotor tip identified by Suder and Celestina[4] in their transonic rotor studies. Therefore, this region can be presumed to be low in velocity and unsteady to the same extent as the shock oscillation. A region of this nature could produce a significant amount of loss and blockage.

The computation did not capture the coherent unsteadiness that was measured behind the shock. One possible reason could be that the frequency of these oscillations was much higher than the computational sample rate could resolve. The frequency of the postshock oscillations may be 15–20 kHz as indicated by Ng and Epstein.[8] It is also possible that the turbulence model used in the computation, although able to simulate the shock motion, is not able to correctly model the viscous interactions that the vortex encounters in a high-gradient region such as a shock. This will be discussed further in the Discussion and Conclusions section.

Another possible reason is that grid density at the shock location and beyond is insufficient. The grid was established to provide the best possible steady results over the complete operating range of the rotor system. It was not optimized for any particular operating condition. For this study the grid may not be fine enough at the shock vortex interaction location to properly capture the discontinuous rise in pressure that occurs in the shock. The pressure rise gradient may not be great enough to cause the unsteadiness seen in the measurements. Additional measured data and computational studies are required to establish the importance of this postshock unsteadiness on rotor performance.

Discussion and Conclusions

The computational and experimental results for the subject rotor both indicated shock oscillation in the blade tip gap region for near-stall operating conditions. Although the computation did not capture all of the features of unsteadiness seen in the measurements, the shock oscillation was well described. The shock oscillation frequency from the computed results was estimated as 2 kHz. It was not possible to resolve frequency from the measurements presented, but the findings from the computational results agree to the same order of magnitude as the levels found in more fundamental studies,[33–35] which relate shock motion to interaction with the blade surface boundary layer. In addition, the frequency agrees well with computed pressure-based oscillations from the shock location to blade trailing edge. The computational sample rate did not allow for investigation of the high-frequency-level oscillations levels of 15–20 kHz as presented by Ng and Epstein.[8] Perhaps the interaction with the clearance vortex drives the higher-frequency oscillations seen in their study. This is a possible cause for the failure of the computation to capture this structure.

Another possible reason for the computation's failure to predict the postshock unsteadiness is the limitations of the turbulence model. The turbulence model must be considered when evaluating the comparisons made in this study. The k-ε turbulence model with a low Reynolds number correction has been tailored for the primary flows that exist in this class of turbomachine. The results from this turbulence model for steady computations have been very good in the prediction of global performance as well as the steady fluid mechanics.[21] The coefficients used in this study to determine the turbulent viscosity, have not been modified from previously established values. The study demonstrates for the first time that the k-ε turbulence model can adequately predict shock system fluctuations that are primarily driven by the interaction with the boundary layer, therefore, indicating that it is properly tailored for this class of flows. Perhaps it requires further tailoring for the swirling flows that exist in a shock/vortex interaction situation. Such an effort is beyond the scope of this study, but certainly should be considered in future work. This study establishes the need to fully evaluate the capabilities of a turbulence model with regard to tip flow unsteadiness prior to full use in design.

From these studies the following conclusions can be drawn:

1) The shock system in this rotor in the absence of an unsteady stator potential field at the near-stall operating condition is unsteady in the relative frame with shock position oscillation levels estimated to be 1–2% of blade chord in the clearance region.

2) Unsteadiness is reduced significantly for operating conditions where the shock is confined to the blade passage.

3) The shock oscillation frequency at the near-stall condition estimated from the unsteady computation was approximately 2 kHz. This is the same frequency that a pressure-based disturbance travels from the shock to the trailing edge and returns.

4) Shock loss was not substantially increased (1%) for the greatest amplitude of shock system oscillation (2%) with the high tip Mach numbers seen in this study. This suggests for this class of rotor, steady codes can be used to assess isolated rotor shock system loss.

5) Further studies, both computationally and experimentally, are required to establish the significance of the measured postshock unsteadiness on performance.

Acknowledgments

The authors acknowledge the management at the U.S. Air Force Wright Laboratory and NASA Lewis Research Center for their support of this research. In addition, the authors would like to acknowledge the support of the General Electric Aircraft Engines Company, who designed the rotor used in this study under U.S. Air Force Contract F33615-83-C-2336. The authors also thank all of the members of the Turbine Engine Division, Compressor Aero Research Lab at Wright–Patterson Air Force Base, U.S. Air Force Wright Laboratory, for their efforts in obtaining the experimental data presented here.

References

[1]Kerrebrock, J. L., "Flow in Transonic Compressors," *AIAA Journal*, Vol. 19, No. 4, 1981, pp. 4–9.

[2]Adamczyk, J. J., Celestina, M. L., and Greitzer, E. M., "The Role of Tip Clearance in High-Speed Fan Stall," *Journal of Turbomachinery*, Vol. 115, No. 1, 1993, pp. 28–39.

[3]Suder, K. L., and Celestina, M. L., "Experimental and Computational Investigation of the Tip Clearance Flow in a Transonic Axial Compressor Rotor," American Society of Mechanical Engineers Paper 94-GT-365, June 1994.

[4]Hah, C., "A Numerical Modeling of Endwall and Tip Clearance Flow of an Isolated Compressor," *Journal of Engineering for Gas Turbines and Power*, Vol. 108, No. 1, 1986, pp. 15–21.

[5]Storer, J. A., "Tip Clearance Flow in Axial Compressors," Ph.D. Dissertation, Cambridge Univ., Cambridge, England, UK, 1991.

[6]Kang, S., and Hirsch, C., "Tip Leakage Flow in a Linear Compressor Cascade," American Society of Mechanical Engineers Paper 93-GT-303, June 1992.

[7]Strazisar, A. J., "Investigation of Flow Phenomena in a Transonic Fan Rotor Using Laser Anemometry," *Journal of Engineering for Gas Turbines and Power*, Vol. 107, No. 2, 1985, pp. 427–435.

[8]Ng, W. F., and Epstein, A. H., "Unsteady Losses in Transonic Compressors," *Journal of Engineering for Gas Turbines and Power*, Vol. 107, No. 2, 1985, pp. 345–353.

[9]Hathaway, M. D., Gertz, J. B., Epstein, A. H., and Straziar, A. J., "Rotor Wake Characteristics of a Transonic Axial-Flow Fan," *AIAA Journal*, Vol. 24, No. 11, 1986, pp. 1802–1810.

[10]Alday, J., Osborne, D. J., Morris, M. B., Ng, W., and Gertz, J., "Flow Randomness and Tip Losses in Transonic Rotors," American Society of Mechanical Engineers, Paper 93-GT-189, June 1993.

[11]Owen, P. R., "Computational Simulation of Unsteady Flow in a Transonic Compressor Rotor," M.S. Thesis, Dept. of Aeronautics and Astronautics, Massachusetts Inst. of Technology, Cambridge, MA, 1986.

[12]Scott, J. N., and Hankey, W. L., Jr., "Navier-Stokes Solutions of Unsteady Flow in a Compressor Rotor," *Journal of Turbomachinery*, Vol. 108, No. 4, 1986, pp. 206–215.

[13]Epstein, A. H., Getz, J. B., Owen, P. R., and Giles, M. B., "Vortex Shedding in High-Speed Compressor Blade Wakes," *Journal of Propulsion and Power*, Vol. 4, No. 3, 1988, pp. 236–244.

[14]Chen, Y. S., "3-D Stator-Rotor Interaction of the SSME," AIAA Paper 88-3095, July 1988.

[15]Erdos, J. I., Alzer, E., and McNally, W., "Numerical Solution of Transonic Flow Through a Fan Stage," *AIAA Journal*, Vol. 15, No. 11, 1977, pp. 1559–1568.

[16]Giles, M. B., "Stator/Rotor Interaction in a Transonic Turbine," AIAA Paper 88-3093, July 1988.

[17]Jorgenson, P. C. E., and Chima, R. V., "An Explicit Runge-Kutta Method for Unsteady Rotor/Stator Interaction," AIAA Paper 88-0049, Jan. 1988.

[18]Rai, M. M., "Navier-Stokes Simulations of Rotor-Stator Interaction Using Patched and Overlaid Grids," AIAA Paper 85-1519, July 1985.

[19]Rao, K., and Delaney, R., "Investigation of Unsteady Flow Through Transonic Turbine Stage," AIAA Paper 90-2408, July 1990.

[20]Law, C. H., and Wadia, A. R., "Low Aspect Ratio Transonic Rotors: Part I—Baseline Design and Performance," *Journal of Turbomachinery*, Vol. 115, No. 2, 1992, pp. 218–225.

[21]Copenhaver, W. W., Hah, C., and Puterbaugh, S. L., "Three-Dimensional Flow Phenomena in a Transonic, High-Through-Flow, Axial-Flow Compressor Stage," *Journal of Turbomachinery*, Vol. 115, No. 2, 1993, pp. 240–248.

[22]Parker, D. E., and Simonson, M. R., "Transonic Fan/Compressor Rotor Design Study, Volume V," U.S. Air Force Wright Aeronautical Lab., TR-82-2017, ADB-69405, Wright–Patterson AFB, OH, Feb. 1982.

[23]Wadia, A. R., and Copenhaver, W. W., "A Numerical and Experimental Investigation of the Effect of Throat Margin and Internal Contraction on Transonic Compressor Performance," American Society of Mechanical Engineers, Paper 94-GT-286, June 1994.

[24]Weyer, H. B., and Hungenberg, H. G., "Analysis of Unsteady Flow in a Transonic Compressor by Means of High-Response Measuring Techniques," CP-177, AGARD, 1975.

[25]Gallus, H. E., Bohn, D., and Broichhausen, K. D., "Measurements of Quasi-Steady and Unsteady Flow Effects in a Supersonic Compressor Stage," *Journal of Engineering for Power*, Vol. 99, No. 3, 1977, pp. 537–544.

[26]Dunker, R. J., and Hungenberg, H. G., "Transonic Axial Compressor Using Laser Anemometry and Unsteady Pressure Measurements," *AIAA Journal*, Vol. 18, No. 8, 1980, pp. 973–979.

[27]Nicholas, D. J., and Freeman, C., "Recent Advances in the Performance of High Bypass Ratio Fans," *Proceedings of the 13th Congress of the International Council of Aeronautics (ICAS)/AIAA Aircraft System and Technology Conference* (Seattle, WA), AIAA, New York, 1982.

[28]Rabe, D. C., Wennerstrom, A. J., and O'Brien, W. F., "Characterization of Shock Wave-Endwall Boundary Layer Interactions in a Transonic Compressor Rotor," *Journal of Turbomachinery*, Vol. 110, No. 3, 1988, pp. 386–392.

[29]Epstein, A. H., Thompkins, W. T., Jr., Kerrebrock, J. L., and Ng, W. F., "Time-Resolved Measurements in a Low-Aspect-Ratio Transonic Compressor Stage," American Society of Mechanical Engineers, Paper 82-GT-201, June 1982.

[30]Sellin, M. D., Puterbaugh, S. L., and Copenhaver, W. W., "Tip Shock Structures in Transonic Compressor Rotors," AIAA Paper 93-1869, July 1993.

[31]Hah, C., "Calculation of Three-Dimensional Viscous Flows in Turbomachinery with an Implicit Relaxation Method," *Journal of Propulsion and Power*, Vol. 3, No. 5, 1987, pp. 415–422.

[32]Puterbaugh, S. L., "Tip Clearance Flow-Shock Interaction in an Advanced, Transonic, Axial-Flow Compressor Rotor," Ph.D. Dissertation, Univ. of Dayton, Dayton, OH, 1994.

[33]McDevitt, J. B., Levy, L., and Deiwert, G., "Transonic Flow About a Thick Circular-Arc Airfoil," *AIAA Journal*, Vol. 14, No. 4, 1976, pp. 606–613.

[34]Lee, B. H. K., "Oscillatory Shock Motion Caused by Transonic Shock Boundary-Layer Interaction," *AIAA Journal*, Vol. 28, No. 5, 1989, pp. 942–944.

[35]Kim, H., Matsuo, K., Kawagoe, S., and Kinosita, T., "Flow Unsteadiness by Weak Normal Shock Wave/Turbulent Boundary Layer Interaction in Internal Flow," *JSME International Journal*, Series II, Vol. 34, No. 4, 1991, pp. 457–465.

[36]Puterbaugh, S. L., and Copenhaver, W. W., "Flowfield Unsteadiness in the Tip Region of a Transonic Compressor Rotor," *Proceedings of Unsteady Flows in Aeropropulsion*, AD-Vol. 40, American Society of Mechanical Engineers, New York, 1994, pp. 77–86.

[37]Cattafesta, L. N., "An Experimental Investigation of Shock Wave/Vortex Interaction," Ph.D. Dissertation, Pennsylvania State Univ., University Park, PA, 1992.